Near-Field Wireless Power Transfer to Embedded Smart Sensor Antennas in Concrete

Xiaohua Jin [1], Juan M. Caicedo [2], and Mohammod Ali [1]

[1] Department of Electrical Engineering
[2] Department of Civil and Environmental Engineering
University of South Carolina, Columbia, South Carolina, 29208, USA
alimo@cec.sc.edu, caicedo@cec.sc.edu

Abstract ─ Wireless power transfer to embedded smart sensor antennas using near-field coupled loop antennas is experimentally studied. Multi-turn loop antennas designed for operation at around 10 MHz show that they can attain fairly high efficiency when properly matched and operated in close proximity to each other whether in free-space or within dry concrete. When one loop is embedded inside 2, 4, and 6 cm of concrete while the other resides over it, it is shown that the embedded loop can receive about 1.9, 1.6, and 1.3 watts of power respectively when the transmit power is 5 watts. Thus, even with an external transmitter with only 1 watt of power (30 dBm) will allow the received power to be 380 mw, 360 mw, and 260 mw for 2, 4, and 6 cm of concrete respectively. It is expected that the use of an even larger loop, magnetic material loading, and or the use of a flux concentrator will increase the efficiency further.

Index Terms ─ Concrete, embedded, near-field, sensor, wireless power.

I. INTRODUCTION

The infrastructure that supports the smooth operation of our society such as, buildings, roads, and bridges has grown in an incredible rate during the last decades. Many of these structures have surpassed their life cycle and require routine structural evaluation to ensure proper operation and safety. In addition, the nation's infrastructure is aging and major upgrades are becoming a necessity. The structural integrity of a building or bridge can be compromised in several ways. For example, the rebar could corrode due to the salt used to de-ice roads, humidity and other environmental factors.

This corrosion reduces the area of the steel bars and it eventually changes the stress distribution within the reinforcement. Structural Health Monitoring (SHM) focuses on developing sensor technologies and systems that assesses the integrity of structures [1]-[10]. Apart from conventional visual inspection [11] and ground penetrating radar (GPR) [12]-[13], various types of sensors have been introduced for SHM applications, such as fiber optics [14], strain gauges [15], accelerometers, guided wave [16]-[18] and ultra sound sensors. Such sensors and the necessary wire connections must be installed while the infrastructure is being built or afterwards as retrofits. The wires connect the sensors with their data acquisition stations to which measured data are collected and processed.

In recent years, there has been a growing interest on wireless sensors for structural health monitoring [19]-[27]. Major advantages of wireless sensors over traditional wired sensors are their low cost and ease of installation. Most of the sensors studied in the literature utilize RF (radio frequency) wireless modules that operate outside the infrastructure, and hence some sort of wired connection to the actual measuring unit (strain gauge, humidity sensor) is required for the data to reach the outside wireless unit.

Wireless sensors that can be embedded or buried within the infrastructure, such as a concrete bridge pier during its construction phase would be clearly a better choice. Wireless embedded sensors will have improved reliability since the lack of any wired connection will prevent the sensor from loss of connection due to crack and corrosion in the wire resulting from changes in the surrounding environment. The possibility of developing such

sensors has been conceptually demonstrated by some RF studies of antennas buried in concrete [28]-[32].

The sensors when placed in appropriate locations of the structure will measure strain, vibration, moisture, etc., and then communicate such data to other sensors and or to a supervisory base station. The sensors will operate independently and will be capable of processing information and make decisions, and hence called *smart sensors*. A basic schematic illustrating a typical sensor deployment scenario is shown in Fig. 1. However, for smart wireless sensors energizing the sensor battery wirelessly from outside is essential because once embedded the sensors cannot be accessed without destroying the structure.
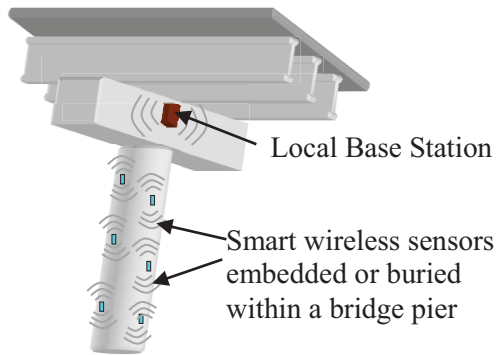
Fig. 1. Proposed distributed embedded or buried wireless sensors within a bridge pier.

In the literature, wireless power transfer has been addressed from two different thrusts: (1) far-field radiated power transfer, and (2) near-field coupled power transfer.

For far-field radiated power transfer, a rectenna [33-35] consisting of an antenna for receiving microwave power, filters, and a diode (mostly Schottky diode) as a rectifying component are needed. The rectenna can receive microwave power and convert it into dc output. Except for difficult to access areas, wireless power transfer using far-field radiated power is very inefficient. For example, in [31] we find that a microstrip patch antenna embedded in 20 mm thick concrete receives only 10.4 mw of power at a distance of 60 cm when the

transmit power is 7w.

Clearly for smart sensors embedded in concrete or other structures, wireless power transfer using near-field coupling will be far more efficient than far field wireless power transfer. For the latter case, just above the surface of the infrastructure closely coupled power transfer antennas and transmit circuits will be installed. The transmit circuits and the external antennas can be energized using solar energy or energy from utilities if available. With the proliferation of RFID (Radio Frequency Identification Device), near-field wireless power transfer has become an intense activity of research and development [36-37], [32] including wireless phone battery charging, car battery charging, etc. The objective of this paper is to study the efficacy of wireless power transfer to sensor elements that can be embedded in concrete.

To that end, a multi-turn loop antenna is designed and matched for operation in free-space. Experiments are performed to evaluate the wireless power transmission loss in free-space for two closely coupled loops. Then wireless power transmission loss when one of the loops is embedded in concrete is measured. Measurements are performed for different thicknesses of concrete demonstrating the feasibility to charge the battery of a wireless embedded sensor in concrete.

II. ANTENNA CONFIGURATION

We consider a square spiral loop printed on one side of a 9 cm by 9 cm by 0.0508 cm Rogers 5880 substrate (ε_r=2.2, tanδ=0.0002).

The back side of the substrate does not contain a ground plane. The end of the inner loop turn is connected to a trace on the back surface of the substrate using a via. The loop geometry is shown in Fig. 2. The antenna is fed using a 50 Ω SMA connector. Three loop configurations were investigated (see Table 1).

Table 1: Square spiral loop configurations studied

Loop Type	Name	Width of Strip (cm)	Gap Between Strips (cm)
1	Thin dense	0.1	0.1
2	Plain	0.2	0.2
3	Thin	0.1	0.3
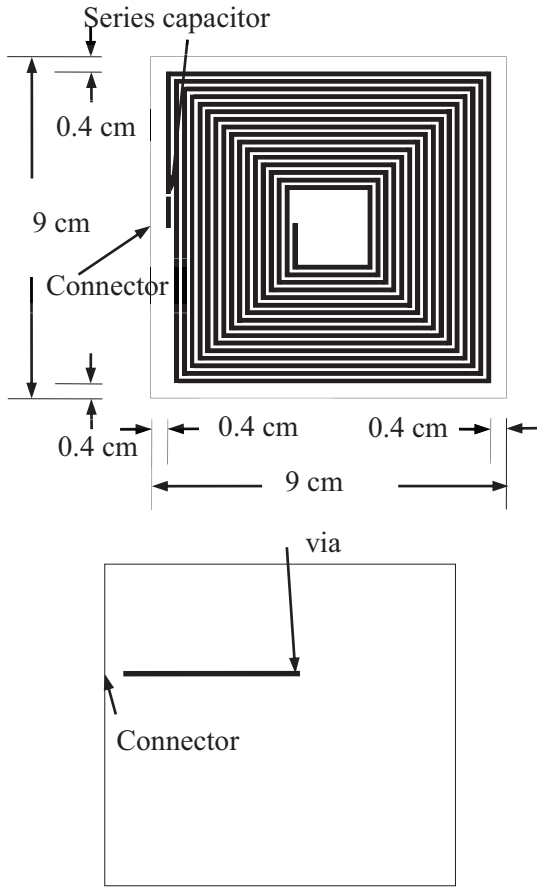
Fig. 2. A multi-turn square spiral loop antenna in free-space with a series chip capacitor. Top and bottom views.

III. SIMULATION RESULTS

Antenna impedance and S-parameters were studied by performing modeling and simulations using Ansys HFSS (High Frequency Structure Simulator). Our objective was to design efficient coupled resonant loop antennas for wireless power transfer where each loop was matched to a 50 Ω feed transmission line. Initially, all simulations were performed at 13.56 MHz. Given the long wavelength (22 meters), the multi-turn loop shown in Fig. 2 is electrically small and thus not self-resonant. In order to force it to resonate at a specific frequency, knowledge about its impedance characteristics is required. Simulated self-resistance data of the three loops listed in Table 1 are plotted in Fig. 3 as function of the number of turns. Clearly, the "Plain" and "Thin" loops have smaller self-resistances which will be difficult to match with a 50 Ω feed transmission line. The self-

resistance of the "Thin dense" loop exceeds 50 Ω when the number of turns exceeds 15. Therefore, for this particular board size if we construct a 16 turn loop with trace width of 1 mm and trace gap of 1 mm that will meet our 50 Ω impedance matching requirements.
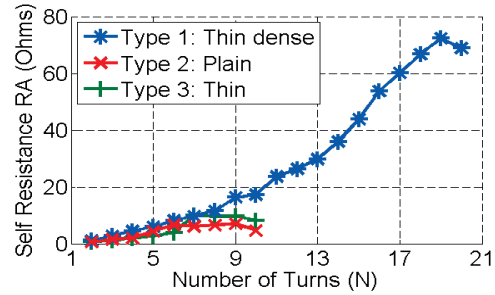
Fig. 3. Simulated loop self-resistance, R_A at 13.56 MHz versus number of turns, N.

Next, we look into the inductance the loop produces. As indicated before, given that this is a magnetic antenna it will have energy stored in its magnetic field which is characterized by its self-inductance. The self-inductances of all three antennas were simulated using HFSS.

Analytically, loop self-inductance is given by [38]:

$$L_{ant} = 2.34\mu_0 N^2 \frac{d_{avg}}{1+2.75p}, \qquad (1)$$

where N is the number of turns and based on the coefficients for modified wheeler expression, for the case "Layout - Square", the layout dependent are 2.34 and 2.75, respectively.

For all three loops listed in Table 1, there are the outer diameter $d_{out} = 0.082$ (m), and the inner diameter $d_{in} = d_{out} - 0.002\,(2N-1)$ (m), $d_{out} - 0.002\,(4N-2)$ (m), and $d_{out} - 0.002\,(4N-3)$ (m) for loops of Type 1, Type 2, and Type 3, respectively, where the average diameter $d_{avg} = \frac{d_{out}+d_{in}}{2}$, fill ratio $p = \frac{d_{out}-d_{in}}{d_{out}+d_{in}}$, and $\mu_0 = 4\pi \times 10^{-7}$ (H/m).

Simulated and calculated (using Eqn. (1)) self-reactance data for these three loops are shown in Fig. 4. Simulated and calculated data are in good agreement for Type 2 and Type 3 loops. For the Type 1 loop (Thin dense), simulated self-reactance is larger than the calculated self-reactance,

especially for larger *N*. The difference between the simulated and calculated reactance of Type 1 for higher *N* is due to the larger parasitic capacitance between two adjacent turns.
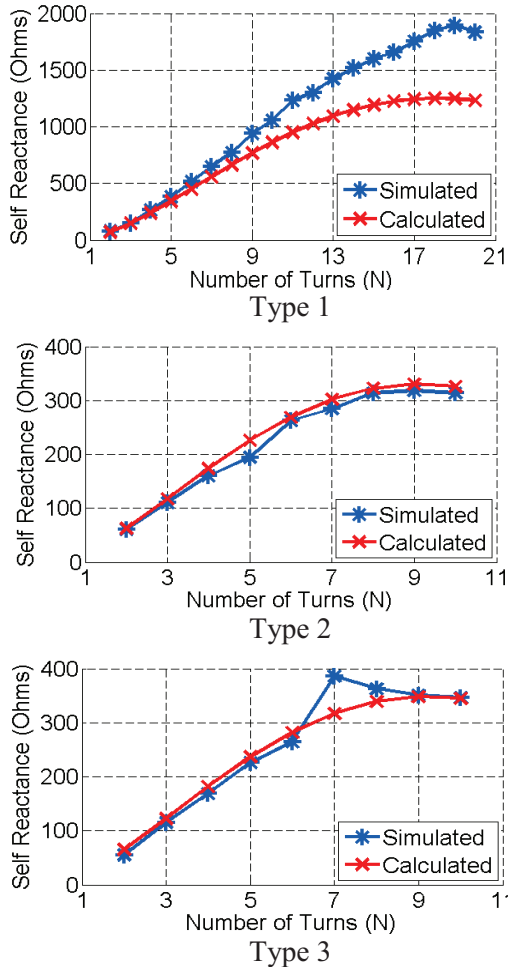
Type 1

Type 2

Type 3

Fig. 4. Simulated and calculated (using Eqn. (1)) loop self-reactance, X_A at 13.56 MHz versus *N* for loops of Type 1, Type 2, and Type 3, respectively.

Comparing the self-impedances of Type 2 and Type 3, it is seen that the Type 1 loop can offer much larger input resistance which will make it easier to match it with a 50 Ω line. For example, for *N* = 16 the Type 1 loop has self-impedance of 53.73+j1656 Ω at 13.56 MHz. Simulated self-resistance and reactance of Type 1 (16-turn loop) are shown in Fig. 5 as function of frequency. Both the self-resistance and reactance increases with frequency as expected. It is clear that antenna resistance variation with frequency is fairly slow and would not be a problem for impedance

matching. However, because the antenna is electrically very small, the inductance varies quite rapidly and thus the matched bandwidth is expected to be narrow
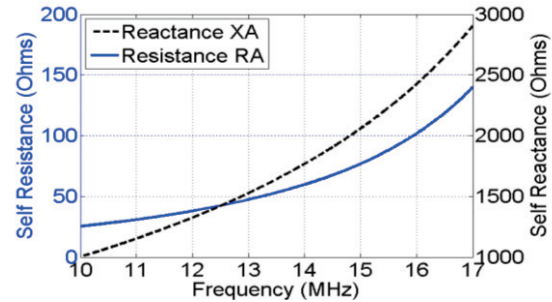
Fig. 5. Simulated self-resistance and reactance of the 16-turn loop versus frequency (MHz).

IV. EXPERIMENTAL RESULTS

A. Free-space measurement results

Figure 6 (a) shows a 16-turn loop that was fabricated on FR4 substrate. Measured S_{11} (dB) data of the loop matched using different chip capacitors are shown in Fig. 6 (b). An Agilent E5071C vector network analyzer (VNA) was used to perform the measurements. It is clear that the tuning frequency can be changed by choosing an appropriate capacitor.
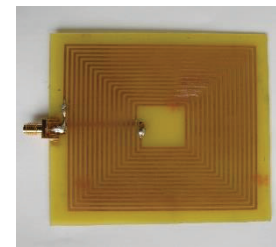
(a)
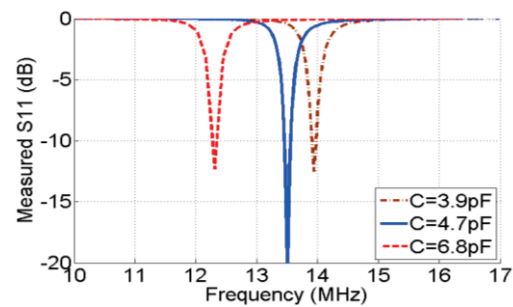
(b)

Fig. 6. Measured S_{11} (dB) data of 16-turn loop versus frequency.

To explore the transmission properties between two resonant loops they were connected to two ports of a VNA and were brought close to each other as shown in Fig. 7 below. Measured S_{11} (dB) data shown in Fig. 8 clearly shows that there are two resonances present when the distance is 3 to 10 cm. Only when the distance is larger (30 cm; i.e., greater than 0.1 wavelength) the double resonance disappears because the coupling between the two loops becomes weaker and the loop behaves like a loop in isolation.
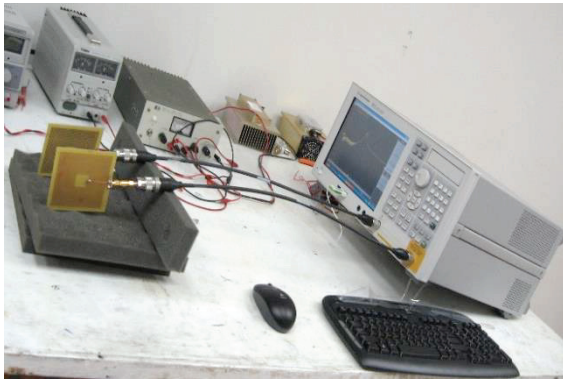
Fig. 7. Measurement setup for two loops in free space.

Measured S_{12} (dB) data for two closely coupled loops at different distances are shown in Figs. 8 (b) and (c). Distance varies as 1 to 5 cm at 1 cm increment and then as 6, 10, 20, and 30 cm. Measured S_{11} (dB) results are shown in Fig. 8 (a), where from it is clear that for 30 cm distance the loop resonance shows a single well-defined resonance that coincides with the resonance of an isolated loop in free-space. As the loops are brought closer and closer mutual coupling increases significantly which is manifested in two resonances.

Measured S_{12} (dB) results show that for distances less than 30 cm the loss is smaller than 10 dB. The (upper or lower) resonant frequencies are listed in Table 2, which will shift according to the relative distance d (cm). As apparent, for larger distances the frequencies are closer and eventually merging, while for very short distances the frequencies significantly diverge from each other.

(a)

(b)

(c)
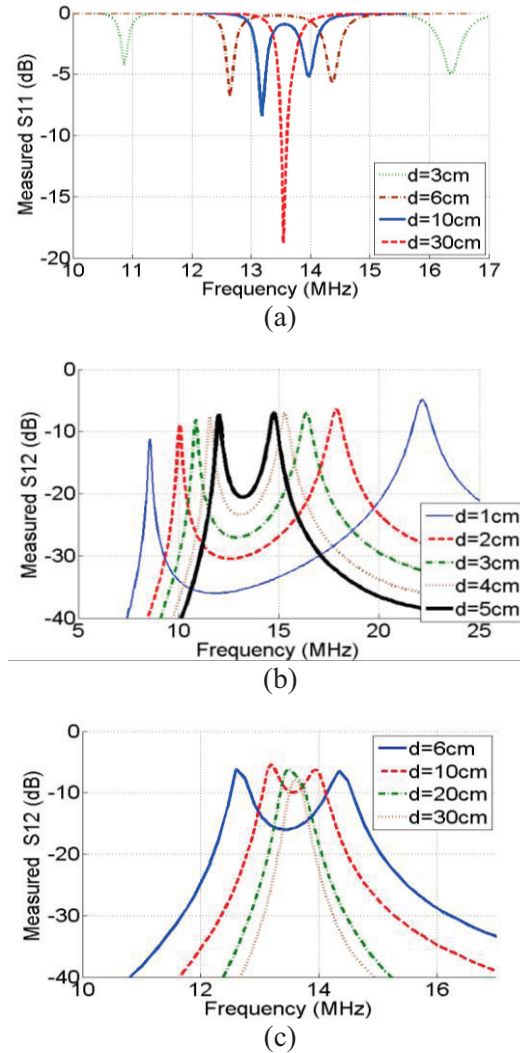
Fig. 8. Measured S-parameters of 16-turn loops at distance, d, in free space, $C = 4.7$ pF.

Table 2: Resonant frequency of two loops in free space.

d(cm)	1	2	3	4	5	6	10	20	30
Lower resonant frequency (MHz)	8.58	10.06	10.86	11.58	12.03	12.64	13.18	13.47	13.54
Upper resonant frequency (MHz)	22.15	17.82	16.36	15.30	14.76	14.37	13.96		

B. Measurement results in concrete

Subsequently measurements were performed when one of the loops were embedded inside concrete. This measurement setup is shown in Fig. 9, where the thickness of each concrete slab is 2 cm. Thus, we have the thickness of concrete: $t = 2$ cm for one layer of concrete, $t = 4$ cm for two layers of concrete, and $t = 0$ for no concrete between (*i.e.,* free space). Measured results according to this situation are shown in Fig. 10.

(a)
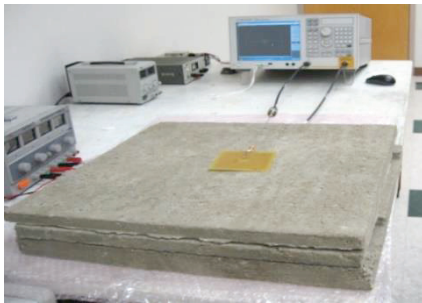
(b)

Fig. 9. Measurement setup: (a) Loop 1 put inside the concrete, and (b) Loop 2 put near concrete.
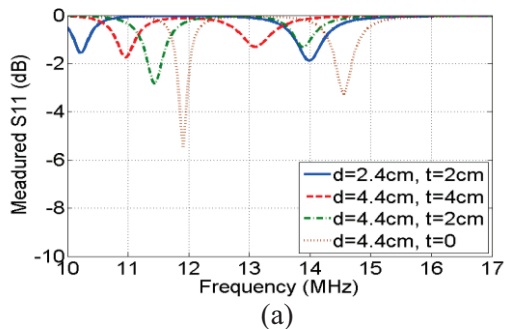
(a)
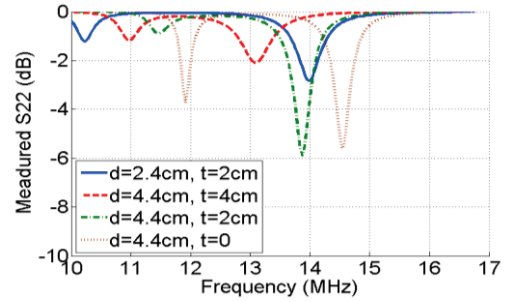
(b)
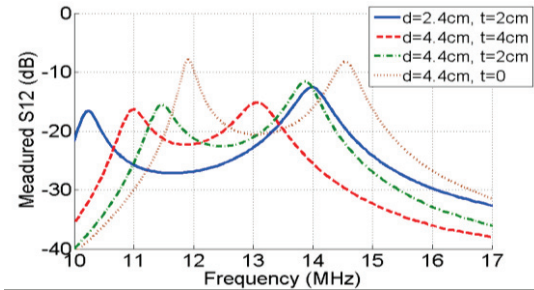
(c)

Fig. 10. Measured S_{11} (dB) for: (a) loop 1 inside concrete, (b) loop 2 touching the surface of concrete with $C = 4.7$ pF at relative distance d with concrete thickness t, and (c) measured S_{12} (dB) or transmission between the two loops.

Clearly for 2 cm of concrete thickness transmission loss is about 12 dB which increases to 15 dB for 4 cm thick concrete. Free-space loss is about 9 dB. Note that, the coupled antenna system has two closely separated resonant frequencies and we are discussing the performance at the higher frequency. Observing the impedance matching of the external and embedded loops, it is apparent that the matching is not good when the antennas are near concrete. To improve the impedance matching, we decided to use $C = 15$ pF instead of 4.7 pF. The measured results comparing these two matching scenarios are shown in Fig. 11. Note that, with $C = 15$ pF the operating frequency is significantly lower (8.5 MHz as opposed to 14 MHz). Because of the improvement in matching transmission, loss even in concrete is much lower (5 dB for 4 cm of concrete).

(a)

(b)

(c)
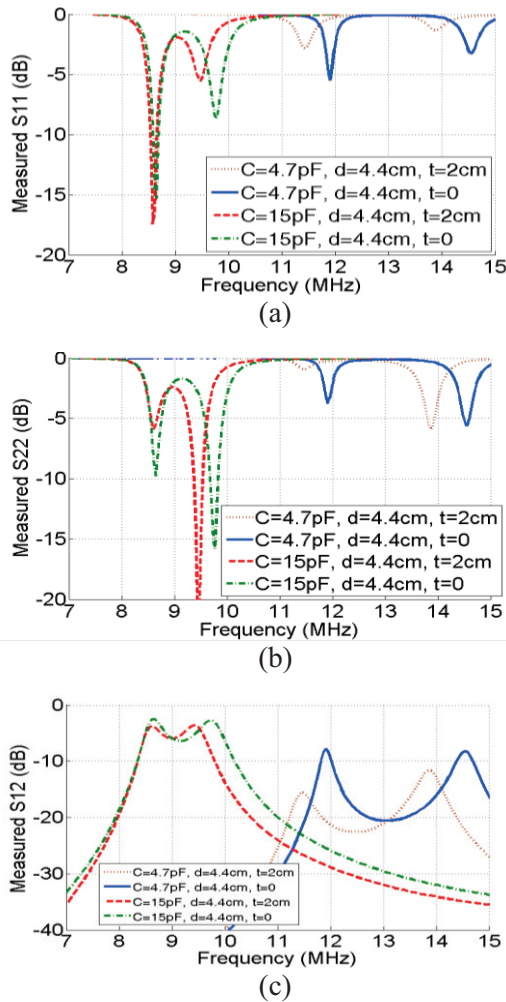
Fig. 11. Measured S₁₁ (dB) and S₁₂ (dB) or transmission for two loops with C = 4.7 and 15 pF at relative distance d with concrete of thickness t between.

V. RECEIVED WIRELESS POWER

Tests were performed using a power meter and a network analyzer to determine the power transmission efficiencies also. In this case, the power received by the embedded antenna was measured using a power meter. The transmit antenna was connected to a vector network analyzer and was set to signal generator mode of operation. These results are shown in dBm scale in Fig. 12 (a) and in watt scale in Fig. 12 (b). The maximum received powers corresponding to 5W of transmit power are 1.9, 1.6 and 1.3W with 2, 4, and 6 cm of concrete thickness respectively. Hence, the corresponding power transmission efficiencies

through concrete are 38%, 32% and 26%, respectively.

(a)

(b)
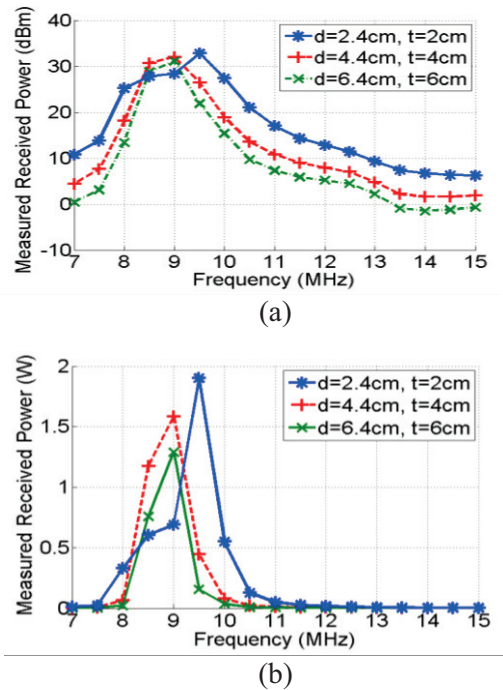
Fig. 12. Measured received power results with input 5W to transmitting loop with series capacitor 15 pF.

VI. CONCLUSION

The concept and prospects of energizing the battery of a wireless sensor embedded in concrete are introduced. It is shown that a well-designed pair of coupled resonant loop antennas operating around 10 MHz can achieve nearly 40% power transfer efficiency even in the presence of 2 cm of concrete. Given the loops operate in very close proximity to each other and that their resonant frequencies are susceptible to slight changes in the distance and the environment, proper matching of their impedance under a deterministic scenario will ensure even higher power transfer efficiency. Nevertheless, wireless embedded sensors that require very small power (10-100 mW) can be easily charged using the proposed scheme where both the embedded and external elements are left unattended and are in essence therefore self-sustained.

ACKNOWLEDGMENT

REFERENCES

[1] S. W. Doebling, C. R. Farrar, M. B. Prime, and D. W. Shevitz, "Damage identification and health monitoring of structural and mechanical systems from changes in their vibration characteristics: a literature review," *Technical Report, Los Alamos National Laboratory*, May 1996.

[2] V. Giurgiutiu and A. Zagrai, "Damage detection in thin plates and aerospace structures with the electro-mechanical impedance method," *Structural Health Monitoring-an International Journal*, vol. 4, pp. 99-118, 2005.

[3] J. M. Caicedo and S. J. Dyke, "Determination of member stiffnesses for structural health monitoring," in *3rd World Conference in Structural Control*, Como, Italy, 2002.

[4] J. M. Caicedo, S. J. Dyke, and E. A. Johnson, "Natural excitation technique and Eigensystem realization algorithm for phase I of the IASC-ASCE benchmark problem: simulated data," *Journal of Engineering Mechanics*, vol. 130, pp. 49-60, 2004.

[5] J. M. Caicedo and S. J. Dyke, "Damage detection on cable-stayed bridges using acceleration measurements," in *7th International Conference on Motion and Vibration Control*, St. Louis, MO, 2004.

[6] J. M. Caicedo and S. J. Dyke, "Experimental validation of structural health monitoring for flexible bridge structures," *J. Struct. Control and Monitoring*, vol. 12, pp. 425-443, 2005.

[7] J. M. Caicedo, N. Catbas, M. Gul, and R. Zaurin, "Phase I of the benchmark problem for bridge health monitoring: numerical data," in *18th Engineering Mechanics Division Conference (EMD2007)*, Blacksburg, Virginia, 2007.

[8] D. Giraldo, J. M. Caicedo, and S. J. Dyke, "Damage detection accommodating varying environmental conditions," *Structural Health Monitoring*, vol. 5, pp. 155-172, 2006.

[9] D. Giraldo, J. M. Caicedo, W. Song, B. Mogan, and S. J. Dyke, "Modal identification through ambient vibration: a comparative study," in *24th International Modal Analysis Conference*, St. Louis, MO, 2006.

[10] J. M. Caicedo, A. Dutta, and B. A. Zarate, "System identification and model updating of the Bill Emerson memorial bridge," in *4th World Conference on Structural Control and Monitoring*, San Diego, CA, 2006.

[11] M. Moore, D. Rolander, B. Graybeal, B. Phares, and G. Washer, "Highway bridge inspection: state of the practice survey," *Federal Highway Administration*, McLean, VA FHWA-RD-01-033, April, 2001.

[12] C. Maierhofer, "Nondestructive evaluation of concrete infrastructure with ground penetrating radar," *Journal of Materials in Civil Engineering*, vol. 15, no. 3, pp. 287-297, May/June 2003.

[13] Ground Penetrating Radar, http://www.geosphereinc.com/gpr_gpradar.html

[14] W. L. Schulz, J. P. Conte, and E. Udd, "Long gauge fiber optic Bragg grating strain sensors to monitor civil structures," *SPIE*, vol. 4330, p. 56, 2001.

[15] T. Nagayama, M. R. Sandoval, B. F. Spencer, Jr., K. A. Mechitov, and G. Agha, "Wireless strain sensor development for civil infrastructure," *Proc., 1st Int. Workshop on Networked Sensing Systems*, pp. 97-100, 2004.

[16] D. N. Alleyne, B. Pavlakovic, M. J. S. Lowe, and P. Cawley, "Rapid long-range inspection of chemical plant pipework using guided waves," *Insight*, 43, pp. 93-96, 2001.

[17] H. Kwun, S. Y. Kim, and G. M. Light, "Long-range guided wave inspection of structures using the magnetostrictive sensor," *J. Korean Soc. NDT*, 21: 383-390, 2001.

[18] J. L. Rose, "Standing on the shoulders of giants: an example of guided wave inspection," *Mat. Eval.*, 60, pp. 53-59, 2002.

[19] J. P. Lynch, K. H. Law, A. S. Kiremidjian, T. Kenny, and E. Carryer "A wireless modular monitoring system for civil structures," *Proceedings of the 20th International Modal Analysis Conference*, Los Angeles, CA, February 4-7, 2002.

[20] J. P. Lynch, "Overview of wireless sensors for real-time health monitoring of civil structures," *Proc. of the 4th International Workshop on Structural Control and Monitoring*, New York City, June 10-11, 2004.

[21] S. W. Arms, J. H. Galbreath, A. T. Newhard, and C. P. Townsend, "Remotely programmable sensors for structural health monitoring," *Structural Materials Technology (SMT): NDE/NDT for Highways and Bridges*, Buffalo, NY, September 16, 2004.

[22] J. P. Lynch, A. Sundararajanb, K. H. Lawb, H. Sohnc, and C. R. Farrarc, "Design of a wireless active sensing unit for structural health monitoring," *SPIE 11th Annual International Symposium on Smart Structures and Materials*, San Diego, CA, USA, March 14-18, 2004.

[23] B. F. Spencer, M. Ruiz-Sandoval, and N. Kurata, "Smart sensing technology: opportunities and challenges," *Structural Control and Health Monitoring*, vol. 11, pp. 349-368, 2004.

[24] D. D. L. Mascareñas, *Development of An Impedance Method Based Wireless Sensor Node for Monitoring of Bolted Joint Preload*, *M.S. Thesis*, University of California, San Diego, 2006.

[25] D. Musiani, K. Lin, and T. Simunic Rosing, "Active sensing platform for wireless structural health monitoring," *Proceedings of the 6th International Conference on Information Processing in Sensor Networks*, pp. 390-399, 2007.

[26] K. C. Lu, Y. Wang, J. P. Lynch, P.Y. Lin, C. H. Loh,

and K. H. Law, "Application of wireless sensors for structural health monitoring, *The 18th KKCNN Symposium on Civil Engineering*, Taiwan, December 2005.

[27] S. Kim, S. Pakzad, D. Culler, J. Demmel, G. Fenves, S. Glasser, and M. Turon, "Health monitoring of civil infrastructures using wireless sensor networks," *Proceedings of the 6th International Conference on Information Processing in Sensor Networks*, pp. 254-263, 2007.

[28] J. T. Bernhard, K. Hietpas, E. George, D. Kuchma, and H. Reiss, "An interdisciplinary effort to develop a wireless embedded sensor system to monitor and assess the corrosion in the tendons of pre-stressed concrete girders," *Proc. IEEE Topical Conf. Wireless Communication Technology*, Honolulu, Hawaii, pp. 241-243, October 2003.

[29] K. M. Z. Shams, M. Ali, and A. M. Miah, "Characteristics of an embedded microstrip patch antenna for wireless infrastructure health monitoring," *IEEE Antennas Propagation Society Int. Symp.*, Albuquerque, NM, July 2006.

[30] K. M. Z. Shams, A. M. Miah, and M. Ali, "Gain and transmission properties of an embedded microstrip patch antenna for structural health monitoring application," *IEEE Antennas Propagation Society Int. Symp.*, Honolulu, Hawaii, June 2007.

[31] K. M. Z. Shams and M. Ali, "Wireless power transmission to a buried sensor in concrete," *IEEE Sensors Journal*, vol. 7, no. 12, pp. 1573-1577, December 2007.

[32] O. Jonah and S. V. Georgakopoulos, "Wireless power transfer in concrete via strongly coupled magnetic resonance," *IEEE Trans. Antennas Propagat.*, pp. 1378-1384, March 2013.

[33] B. Strassner and K. Chang, "5.8-GHz circularly polarized dual-rhombic-loop traveling-wave rectifying antenna for low power-density wireless power transmission applications," *IEEE Trans. Microwave Theory Tech.*, vol. 51, no. 5, pp. 1548-1553, May 2003.

[34] M. Ali, G. Yang, and R. Dougal, "A new circularly polarized rectenna for wireless power transmission and data communication," *IEEE Antennas Wireless Propagat. Lett.*, vol. 4, pp. 205-208, 2005.

[35] M. Ali, G. Yang, and R. Dougal, "Miniature circularly polarized rectenna with reduced out-of-band harmonics," *IEEE Antennas Wireless Propagat. Lett.*, vol. 5, pp. 107-110, 2006.

[36] K. Finkenzeller, *RFID Handbook*, Second Edition, John Wiley and Sons Inc., 2003.

[37] M. Ali, J. M. Caicedo, and X. Jin, *Wireless Power Transfer to Embedded Sensors*, US Patent Application Number: 20110287713, 2009.

[38] S. S. Mohan, M. del Mar Hershenson, S. P. Boyd, T. H. Lee, " Simple accurate expressions for planar spiral inductances," *IEEE J. of Solid-State Circuits*, vol. 34, no. 10, pp. 1419-1424, October 1999.

Xiaohua Jin received the B.S. and M.E. degrees in Electrical Engineering from Automation Department, Tsinghua University in 1986 and 1989, respectively. She earned the Ph.D. in Mathematics in 2005 and Ph.D. in Electrical Engineering in 2011, both from University of South Carolina, USA. From 2011 to 2014, Jin has been an Assistant Professor at Allen University, South Carolina.

Juan Caicedo is an Associate Professor in the Department of Civil and Environmental Engineering at the University of South Carolina. He received his B.S. in Civil Engineering from the Universidad del Valle in Colombia, South America in 1998. He received his M.S. in 2002 from Washington University in St. Louis and his D.Sc. in 2003 from the same institution. His research interests are in structural dynamics, model updating, structural health monitoring and engineering education. Caicedo is the recipient of the 2009 National Science Foundation CAREER award and has authored and co-authored over 100 conference and journal publications.

Mohammod Ali received the B.Sc. degree in Electrical and Electronic Engineering from the Bangladesh University of Engineering and Technology, Dhaka in 1987, and the M.A.Sc. and Ph.D. degrees, both in Electrical Engineering, from the University of Victoria, Victoria, BC, Canada, in 1994 and 1997, respectively. From January 1998 to August 2001, he was with Ericsson Inc., Research Triangle Park, NC. Since August 2001, he has been with the Department of Electrical Engineering, University of South Carolina at Columbia where currently he is a Professor. Ali is the recipient of the 2003 National Science Foundation Faculty Career Award. He is the author/co-author of over 150 publications and 8 US patents. His research interests include smart antennas, metamaterials and metasurfaces, conformal antennas, and wireless power transfer and wireless sensors.